

Dynamic analysis of guideway structures by considering ultra high-speed Maglev train-guideway interaction

Myung-Kwan Song[†]

*Renewable Energy Development Team, Corporate R&D Institute, Doosan Heavy Industries & Construction,
463-1 Jeonmin-dong, Yuseong-gu, Daejeon 305-811, Korea*

Yozo Fujino[‡]

Department of Civil Engineering, The University of Tokyo, Tokyo 113-8656, Japan

(Received January 9, 2007, Accepted April 1, 2008)

Abstract. In this study, the new three-dimensional finite element analysis model of guideway structures considering ultra high-speed magnetic levitation train-bridge interaction, in which the various improved finite elements are used to model structural members, is proposed. The box-type bridge deck of guideway structures is modeled by Nonconforming Flat Shell finite elements with six DOF (degrees of freedom). The sidewalls on a bridge deck are idealized by using beam finite elements and spring connecting elements. The vehicle model devised for an ultra high-speed Maglev train is employed, which is composed of rigid bodies with concentrated mass. The characteristics of levitation and guidance force, which exist between the super-conducting magnet and guideway, are modeled with the equivalent spring model. By Lagrange's equations of motion, the equations of motion of Maglev train are formulated. Finally, by deriving the equations of the force acting on the guideway considering Maglev train-bridge interaction, the complete system matrices of Maglev train-guideway structure system are composed.

Keywords: magnetic levitation train; Maglev train-guideway interaction; guideway structures; dynamic analysis; finite element analysis.

1. Introduction

Recently, the concern about the feasibility of magnetic levitation train (here after, Maglev train) is being increased all over the world. In 1960's, the development of Maglev train had already commenced in Japan and Germany, where experimental lines were constructed and many field experiments were performed. Nowadays, the construction of commercial lines is being considered in Japan and Germany. In 2004, the line connecting Shanghai with Pudong in China had been constructed, where Transrapid08 (Germany) is being operated at the commercial speed of 430 km/h (Esveld 2001). In Japan, the unmanned ML500 in Miyazaki line set the record for the speed of 517 km/h in 1979. Since 1997, Yamanashi testing line had been built newly, in which various

[†] Principal R & PD Engineer, Ph.D., Corresponding author, E-mail: y13285@yooshin.co.kr

[‡] Professor, Ph.D., P.E.

experiments have been made through driving Maglev train. The manned MLX-01 with five-car formation set the record for the speed of 552 km/h in 1999. In addition, the manned MLX-01 with three-car formation set the best record for the speed of 581 km/h in 2003 (Sogabe *et al.* 2003).

For the feasibility of ultra high-speed Maglev transport system, civil engineers, electrical engineers, and mechanical engineers must do the design, manufacturing, and construction of guideway structures, Maglev train, and super-conducting magnet (hereafter, SCM) without defects. Among these terms, civil engineers must design and construct the guideway structures with the structural safety and aesthetical beauty, of which the structural safety is directly related to human life and so very important factor to be considered. Guideway structures must have not only the structural safety for traffic load, earthquake load, and thermal load, but also the dynamic serviceability for the vibration when Maglev train passes. To get the objective numerical data for this purpose, the numerically accurate analysis model of guideway structures considering Maglev train-guideway interaction must be developed.

The dynamic response prediction of railway bridges subjected to high-speed train loading is complicated in nature, because the dynamic behavior of a bridge induced by the train moving on it is influenced by the interaction not only between the train and bridge, but also between components of a train itself. Recently, many researchers pay attention to the increase of the operating speed of a train. As the operating speed of a train reaches 300 km/h or more, it becomes the more important factor to consider accurately the train-bridge interaction for the design of a bridge. Many researchers contributed to the analytical advancement of this field. Tanabe *et al.* (1997) developed the three-dimensional analysis program for the dynamic interaction analysis of Shinkansen trains and railway bridges. Park (1999) proposed the high-speed train models with seventeen degrees of freedom (hereafter, DOF) and 38 DOF and applied those models to the analysis of railway bridges. Kim *et al.* (1999) fulfilled the parametric study by means of the three-dimensional refined high-speed train model. Song *et al.* (2001, 2003) proposed the simplified three-dimensional analysis method, sub-structuring method, and full 3-dimensional analysis method for the dynamic analysis of high-speed railway bridges. Kwark *et al.* (2004) performed experimental and theoretical studies to determine the dynamic behavior of bridges crossed by a high-speed train. Xia *et al.* (2003) proposed a dynamic analysis model of the bridge-articulated vehicle system, which is composed of the articulated vehicle element model and three-dimensional bridge model, and investigated the vibration of the train and bridge.

As mentioned above, many researchers carried out the dynamic analysis method of railway bridges considering the high-speed train-bridge interaction all over the world. The researchers performed the analysis of Maglev-train guideway interaction in USA, Japan, and Germany. Particularly, Sogabe *et al.* (2003) proposed the vehicle model of Maglev train MLX-01 in Yamanashi testing line and the three-dimensional analysis model of guideway structures, which were modeled by beam elements. By using these models, they proposed the dynamic interaction analysis scheme and investigated the characteristics of the dynamic response of guideway structures. The model in this research was 3-dimensional frame model, and the refined and various 3-dimensional finite elements were not applied to model complicate guideway structures.

In this study, the new three-dimensional Maglev train model and guideway structure model are proposed. By using these models, the dynamic analysis scheme considering Maglev train-guideway interaction is proposed. Based on these models and analysis scheme, the finite element analysis program is developed and the validities of this program are verified through numerical examples. The existing non-conforming flat shell (hereafter, NFS) finite elements (Choi *et al.* 2001) are used

to model the bridge deck of bridges. Therefore, the analysis of bridge decks can be accurate because NFS finite elements with six DOF are very useful to accurately model the folded plate structures like box-type girders. To model the sidewalls of guideways, three-dimensional beam finite elements are used. To model the beam connecting sidewalls and bridge decks, spring connecting elements are used. To model the levitation and guidance force between the super-conducting magnet (hereafter, SCM) and sidewalls, the concept of the equivalent spring model is applied.

2. Operating principles of Maglev train

2.1 Super-conducting magnet

Maglev train can be levitated by the use of the SCM, in which super-conducting phenomena is applied. Super-conducting phenomena means the state that special metals have no electrical resistance for the direct current when they are refrigerated under the specific temperature. Therefore, the special metals have no energy loss, which are expressed as the emission of heat, light, and so on. Therefore, if the coils which are made of such metals are passed through by electrical current,

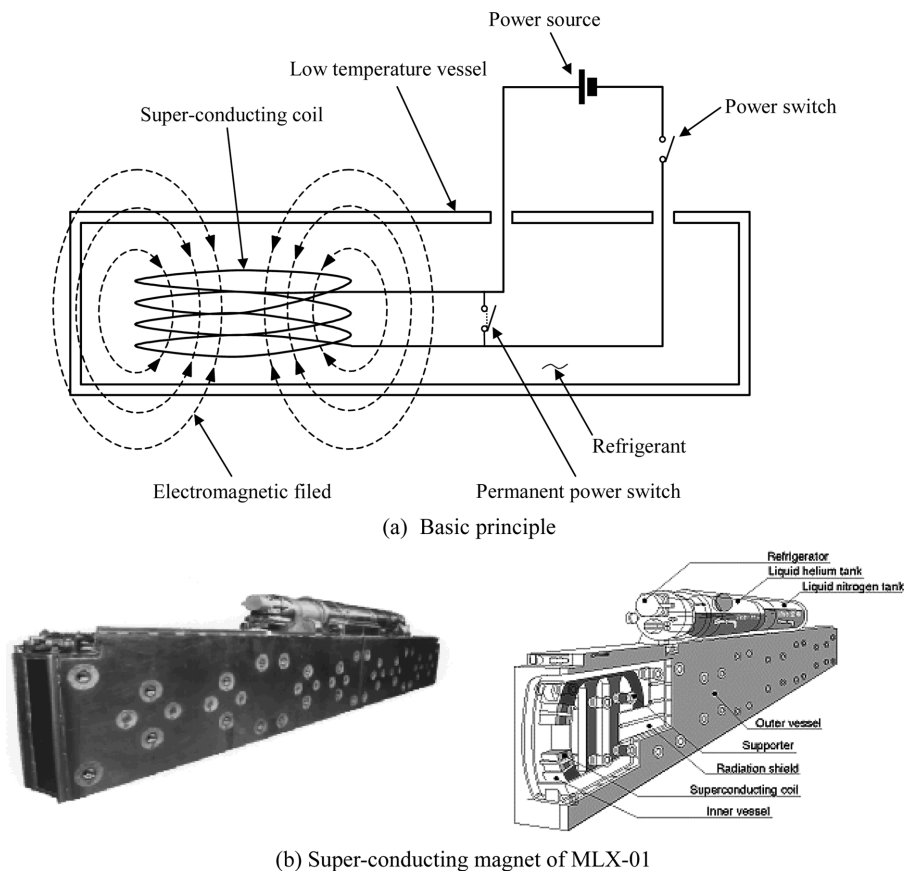


Fig. 1 Principle of super-conducting magnet

they have the permanent electrical fields without the continuous supply of electrical power (Kim 1997).

In Japanese super-conducting magnetic levitation transport system, the coils, which are made of the alloy of Niobium and Titanium (Nb_3Ti) and cooled down under -269°C to get the permanent electrical fields, are installed on Maglev train to fulfill the function of SCM. The attractive and repulsive force between the installed SCM and coils established on the sidewalls of guideways are used to function the levitation, guidance, and propulsion force to incarnate the magnetic levitation transport system. To make a progress practicable, Railway Technical Research Institute (RTRI) in Japan carried out the related researches (Sogabe *et al.* 2003).

2.2 Principles of the propulsion, levitation, and guidance of Maglev train

When Maglev train with SCM passes on the sidewalls of guideways, the electrical current is generated in the coils installed on sidewalls. Therefore, the electrical current is generated in the coils on guideways and the electrical fields of pole-N and pole-S are formed in the coils. At the same time, the attractive force is generated between the different poles and the repulsive force is between the same poles. As a result, Maglev train moves forward by using the attractive and repulsive force. As a matter of course, Maglev train must move forward with the wheels installed at the bottom of a carbody to a certain speed. The coils established on the left and right sides of sidewalls are mutually connected with electric power cables. Therefore, if a carbody leans toward

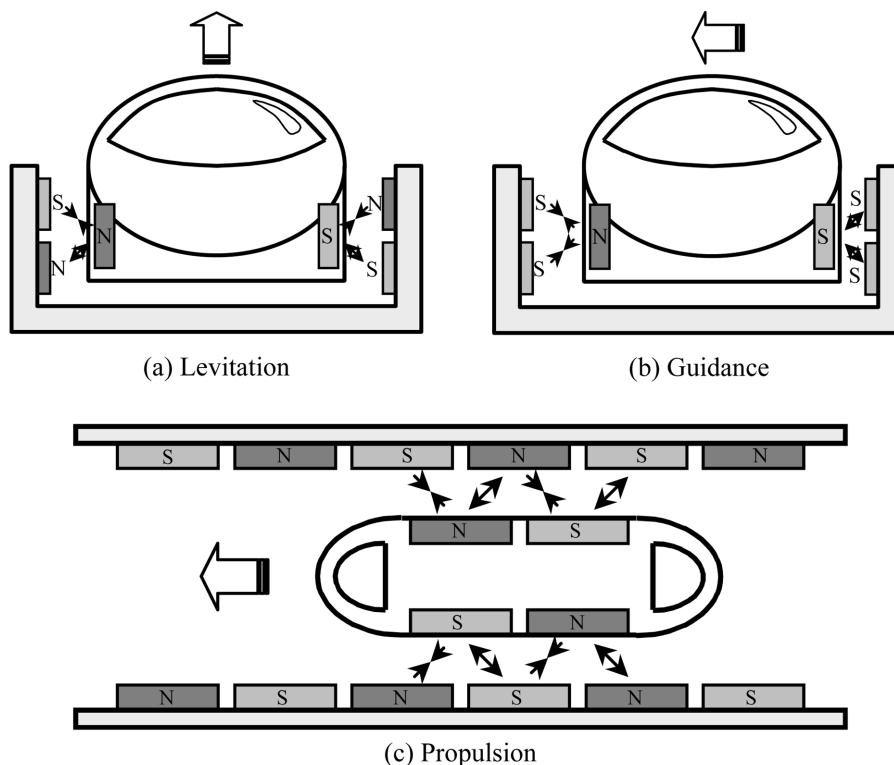
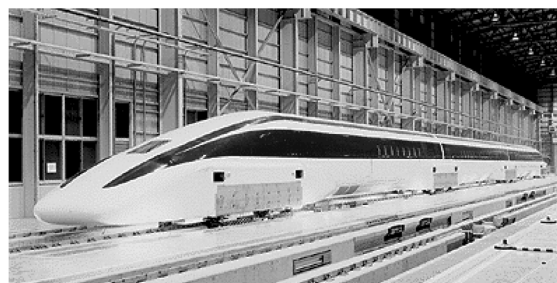
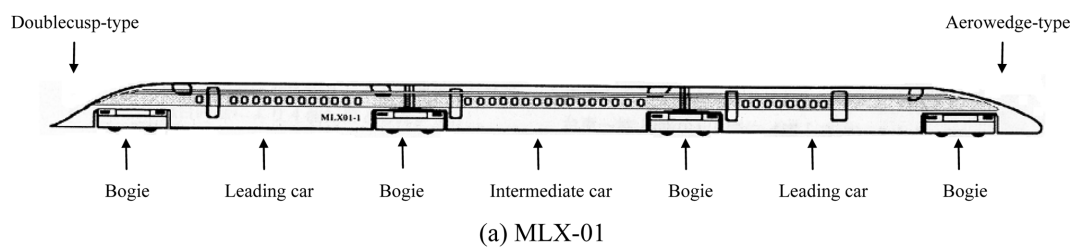


Fig. 2 Principle of Maglev train

one side from the central position of the guideway, the attractive force is formed on the part distant from the sidewall and the repulsive force is on the part near to the sidewall. In other words, a carbody always comes back to the central position of the guideway whenever a carbody leans toward one side.

3. Maglev train model

The first version of MLX-01 of Japanese Maglev train is the articulated bogie system and has three-car formation, i.e., three cars and four bogies (Fig. 3). The second version of MLX-01 has five-car formation, i.e., five cars and six bogies. MLX-01 can run magnetically at the speed of 500 km/h (maximum speed is 550 km/h). The power brake is used as the usual brake system and the disk and air brake are set up as the backup system for urgent times (Yoshioka *et al.* 1998). In Fig. 4, the cross-sectional view of ultra high-speed Maglev transport system including the levitation coils and linear synchronous motor (hereafter, LSM) primary coils is shown. The main three-type



(b) Aerowedge-type leading car



(c) Doublecusp-type leading car

Fig. 3 MLX-01 of ultra high-speed Maglev train

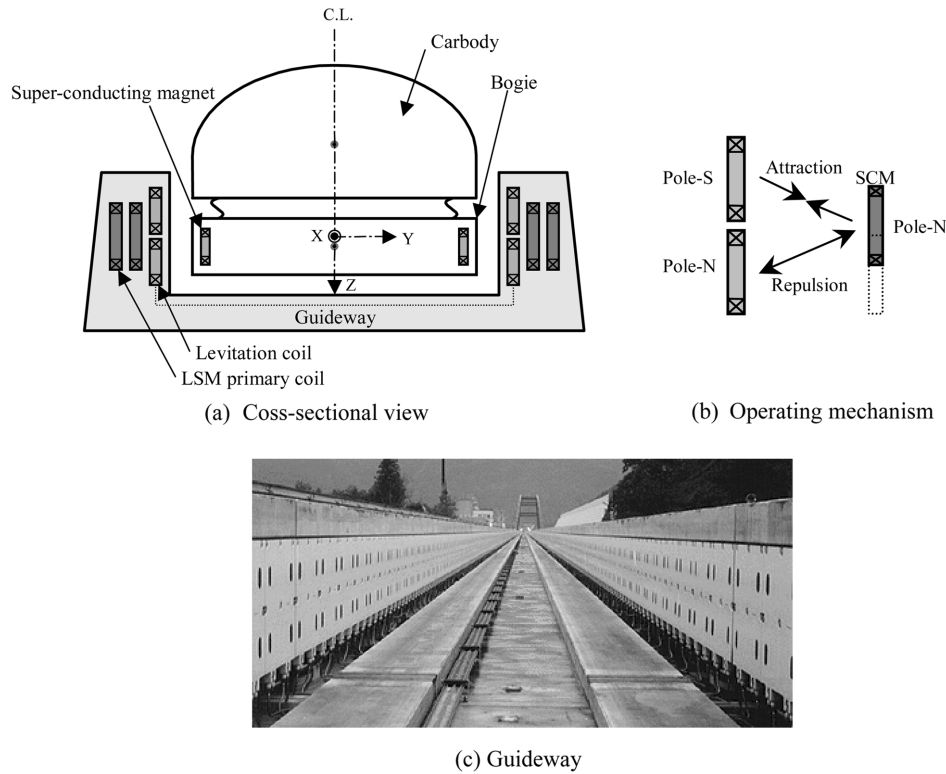


Fig. 4 Transport system of Maglev train

coils of LSM are installed on the inner and outer part of sidewalls. To connect the levitation coils on the sidewalls of both sides, the null-flux cable is used (Higashi *et al.* 1999, Ohashi *et al.* 2000). By the function of the null-flux connection, the electrical currents and magnetic force are generated according to the position and speed of SCM installed on a bogie. When SCM moves under the central position between the upper and lower levitation coils on the sidewall, the repulsive force is generated between the super-conducting coils and lower levitation coils, and the attractive force is generated between the super-conducting coils and upper levitation coils. As a result, the levitation force is generated between the super-conducting coils of SCM and levitation coils of sidewall. By the same way, the guidance force is generated and keeps a car body from straying out of the central position. The super-conducting coils of sidewalls are used not only as the SCM of the levitation and guidance system but also as the secondary LSM. In the system of MLX-01, there are eight pieces of SCM per a bogie.

3.1 Maglev train model

In this study, the Maglev train model is proposed, which has twenty-four DOF, i.e., the six DOF of a carbody, the six DOF of a bogie, and the three DOF of the corporate body of SCM and frame structures (Figs. 5 and 6) (Yoshioka 1988). The six DOF of a carbody mean the sliding motion, swaying motion, bouncing motion, pitching motion, rolling motion, and yawing motion of a carbody $(x_c, y_c, z_c, \theta_c, \phi_c, \varphi_c)$. The six DOF of a bogie mean the sliding motion, swaying

motion, bouncing motion, pitching motion, rolling motion, and yawing motion of a bogie ($x_t, y_t, z_t, \theta_t, \phi_t, \varphi_t$). The three DOF of the corporate body of SCM and frame structures mean the bouncing motion, pitching motion, and rolling motion of the corporate body of SCM and frame structures (z_s, θ_s, ϕ_s). As a result, by applying the Lagrange's equations of motion, the equations of motion of leading and intermediate cars can be derived respectively. Therefore, by superposing these equations of motion, the equations of motion of the multi-link Maglev train can be composed. The dynamic properties and dimensions of Maglev train used in numerical examples are as shown in Tables 1 and 2 (Azakami 1996, Higashi *et al.* 1999, Matsudaira and Takao 1994, Ohashi *et al.* 1998, Ohashi *et al.* 2000, Takao *et al.* 1996).

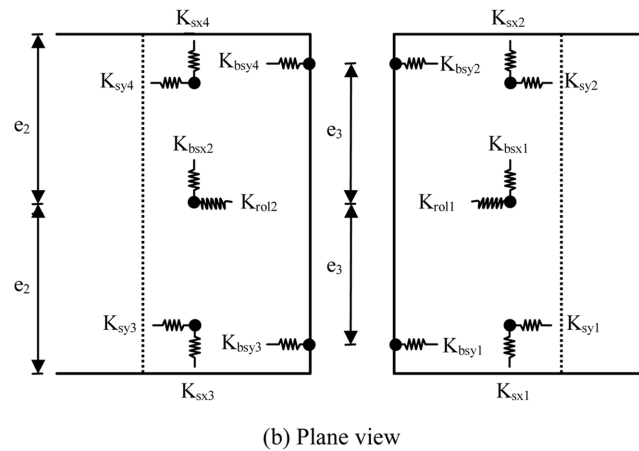
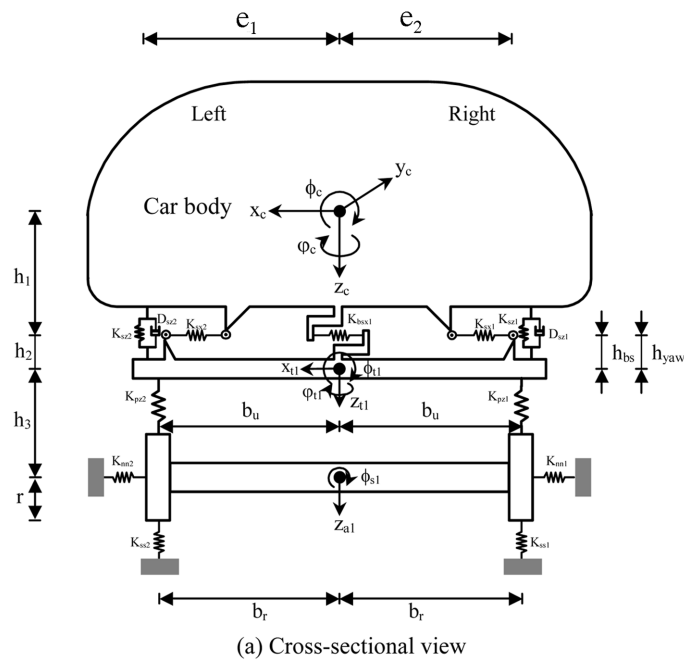


Fig. 6 Three-dimensional model of the coupling part between bogie and carbody

Table 1 Dynamic properties of Maglev train used in the mechanical model

Terms	Symbol	Unit	Value
Carbody mass	m_B	kg	1.37×10^4
Carbody inertia moment	Rolling $I_{B\phi}$	$\text{kg} \cdot \text{m}^2$	1.977×10^4
	Pitching $I_{B\theta}$	$\text{kg} \cdot \text{m}^2$	9.351×10^5
	Yawing $I_{B\psi}$	$\text{kg} \cdot \text{m}^2$	15.85×10^5
Bogie mass	m_T	kg	6.3×10^3
Bogie inertia moment	Rolling $I_{T\phi}$	$\text{kg} \cdot \text{m}^2$	1.634×10^3
	Pitching $I_{T\theta}$	$\text{kg} \cdot \text{m}^2$	1.480×10^3
	Yawing $I_{T\psi}$	$\text{kg} \cdot \text{m}^2$	1.785×10^3
SCM mass	m_S	kg	2.8×10^3
SCM inertia moment	Pitching $I_{S\theta}$	$\text{kg} \cdot \text{m}^2$	5.103×10^3
	Rolling $I_{S\psi}$	$\text{kg} \cdot \text{m}^2$	1.16×10^4
Pneumatic spring	Y K_{sy}	N/m	2.25×10^5
	X K_{sx}	N/m	2.25×10^5
	Z K_{sz}	N/m	1.96×10^5
Bogie vertical damper	D_{sz}	N·s/m	2.45×10^3
Anti-rolling spring	K_{rol}	N/m	3.8×10^4
Bogie lateral stopper spring	K_{bsx}	N·s/m	3.107×10^5
Bogie longitudinal anchor spring	K_{bsy}	N/m	4.9×10^5
SCM vertical spring	K_{pz}	N/m	1.225×10^5
Spring between carbodies	K_{cz}	N/m	4.9×10^5

Table 2 Dimensions of Maglev train used in the mechanical model

Terms	Symbol	Unit	Value
Carbody	Aerowedge-type L_1, L_2	m	10.8, 10.8
	Intermediate L_1, L_2	m	10.8, 10.8
	Doublecusp-type L_1, L_2	m	10.8, 10.8
Bogie	d_1	m	2.025
	d_2	m	2.025
	e_1	m	1.95
	e_2	m	1.75
	e_3	m	1.75
	b_u	m	2.035
	h_1	m	1.4
	h_2	m	0.48
	h_3	m	0.1
	h_4	m	1.3
	h_5	m	0.8
	r	m	0.35
	h_{bs}	m	0.4
h_{ytw}	m	0.4	
SCM	b_r	m	2.98/2
	a	m	1.35
Gap between carbodies	g	m	0.6

3.2 Equations of motion of ultra high-speed Maglev train

To derive the equations of motion of the multi-link Maglev train, the equations of kinematic energy, potential energy, and damping energy of all cars are substituted for the Lagrange's equations of motion. In general, to derive the equations of motion of complex system, the Lagrange's equations of motion based on the analytical dynamics are used as

$$\frac{d}{dt} \left(\frac{\partial E_k}{\partial \dot{q}_v} \right) - \frac{\partial E_k}{\partial q_v} + \frac{\partial E_p}{\partial q_v} + \frac{\partial E_d}{\partial \dot{q}_v} = 0 \quad (1)$$

where $\{q_v\}$ is the DOF of Maglev train. Therefore, the equations of motion of cars are expressed by the DOF of carbodies, bogies, SCM, and a bridge (Appendix A).

Maglev train is the multi-link train, which has the bogie at the connecting part between two carbodies. Therefore, the behavior of carbodies is influenced by the behavior of bogies. As a result, by using the equations of motion of all cars, the system matrices of Maglev train, which are mass matrices, stiffness matrices, damping matrices, and load vectors, can be composed.

4. Guideway structure model

4.1 Three-dimensional model of guideway structures

The guideway structures of Maglev train are composed of the guideways and sub-structures as shown in Fig. 7. To investigate accurately the dynamic behavior of the structural constituents of guideway structures, the dynamic analysis system considering the three-dimensional Maglev train-guideway interaction must be used. In this study, to model the guideway structures in three-dimensional space, the decks, sidewalls, and springs constituting guideway structures are modeled by the various proper finite elements to calculate the structural behavior of constituents accurately.

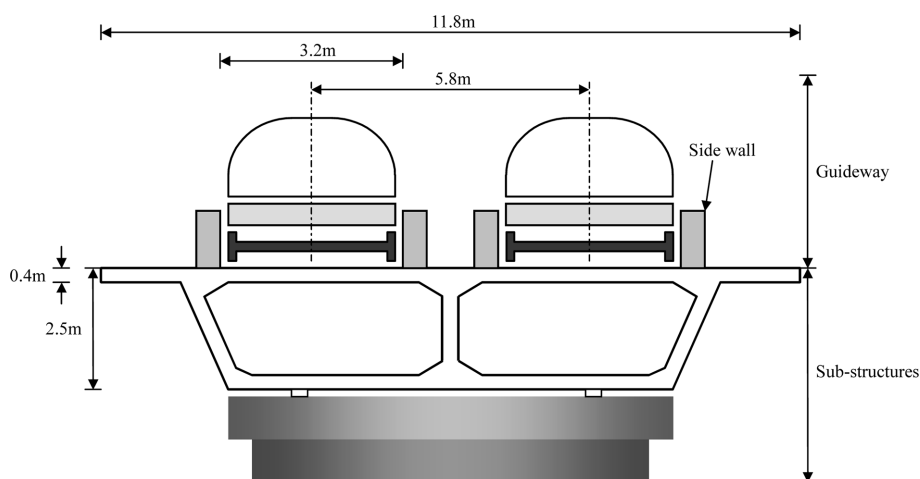


Fig. 7 Structural components of guideway structures

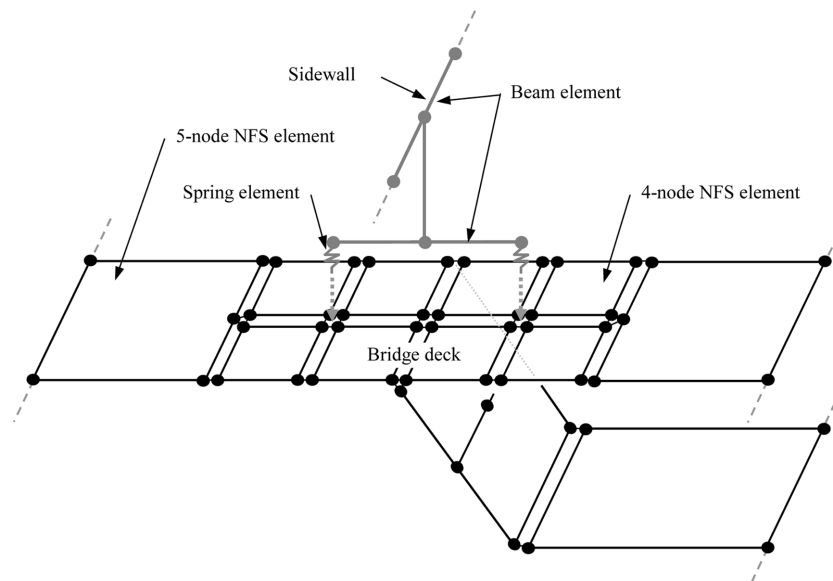


Fig. 8 Three-dimensional model of guideway structures

4.2 Modeling of bridges

In this study, NFS finite element, which can be applied to the adaptive mesh refinement, is used to model the deck of a bridge. NFS finite element has the six DOF per a node including the drilling DOF and can be usefully used to model the folded plate structures like box-type girders, in which the in-plane and out-of-plane deformations are coupled. In the analytical formulation of NFS finite element, the behavior of the element is enhanced by adding the non-conforming mode and by using the direct modification method to pass the patch test (Choi *et al.* 2001). In addition, it is assumed that the in-plane and out-of-plane DOF in NFS finite element are independent. Therefore, the stiffness matrix of NFS finite element is made by assembling the stiffness matrix of plate bending element with stiffness matrix of membrane element. The stiffness matrix obtained through the foregoing procedure is modified by the rigid link correction method to be accurately applied also in the case of the warped geometry of an element. The mass matrix of NFS finite element is made by the HRZ lumping scheme and the inertia moment for rotational DOF is neglected.

4.3 Modeling of sidewalls

Guideways are composed of sidewalls, rigid beams, and rubber bearings as shown in Fig. 9 and these structural constituents are specifically modeled by various finite elements. Three-dimensional beam elements are used to model sidewalls and rigid beams, and spring elements are used to model rubber bearings. When Maglev train moves on guideways, the altitude of SCM passing on sidewalls is variable according to the intensity of levitation force. In this study, it is assumed that SCM keeps the altitude of the sectional centroid of sidewalls.

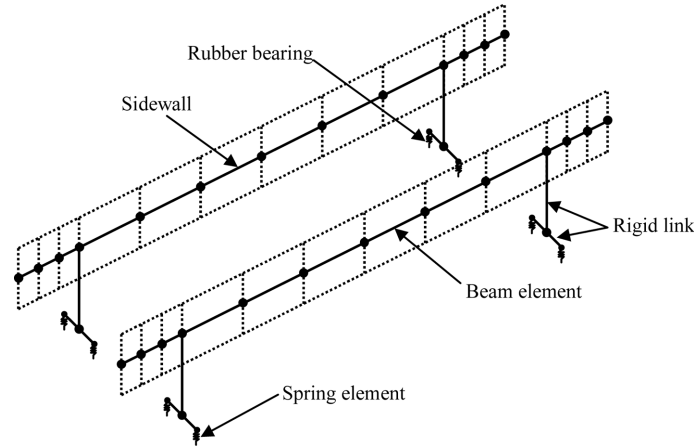


Fig. 9 Model of guideways

4.4 Generation of the roughness profile of sidewalls

Guideways generally have the geometrical uncertainties in vertical and lateral direction, which affect the dynamic response of guideway structures due to the passing train. These uncertainties must be handled numerically following the general procedure of random sampling. To define the roughness profile along the passing distance of SCM, the power spectral density (PSD) function should be assumed. The roughness profile is considered through the stationary and ergodic process in the space, i.e., the random functions in the passing distance x , and are characterized most frequently by PSD function $S(\gamma)$. The PSD function depends on the wave number (γ), which is expressed as shown in Eq. (2).

$$\gamma = \frac{1}{\lambda} = \frac{1}{VT} = \frac{\omega}{2\pi} \quad (2)$$

where λ is the wave length, T is the period of wave, V is the vehicle speed, and ω is the circular frequency of wave.

The PSD function for the generation of roughness, which was proposed by RTRI in Japan through the linear survey of Yamanashi test line, is shown in Fig. 10 (Matsuura *et al.* 1994). In this study, the PSD function of Fig. 10 is used to generating the roughness profile of guideways. The roughness profiles in vertical and lateral direction are generated with substituting the PSD function for Eq. (3).

$$z(x) = \sum_{i=1}^N \sqrt{4S_z(\gamma_i)\Delta\gamma} \cos(2\pi\gamma_i x - \beta_i) \quad (3)$$

where x is the passing distance, N is the number of spectrum to be considered, and β_i is the phase angle distributed between 0 and 2π randomly. In this study, it is assumed that N is 1024 and λ is the value between 1.8 m and 1000 m (Garg and Dukkipati 1984).

The roughness profiles in vertical and lateral direction generated through the foregoing process are given in Fig. 11. Because the roughness profiles are different for each sidewall, the roughness profiles are generated differently for each sidewall by use of the different seed number in random sampling.

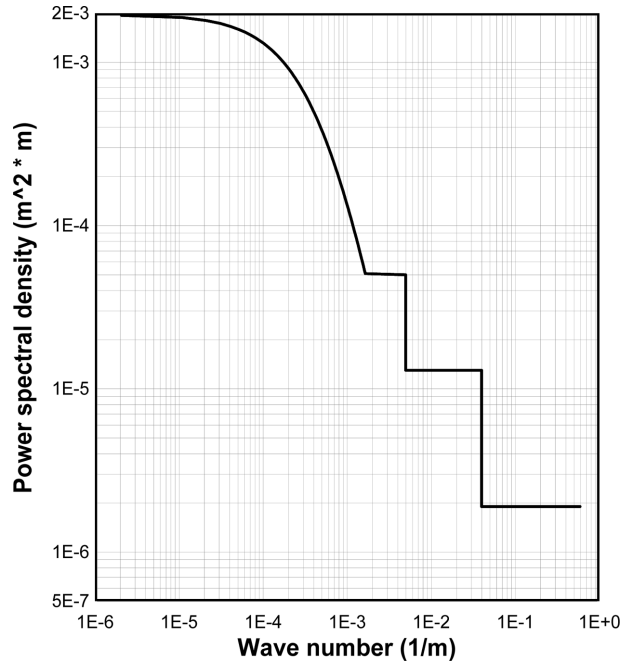
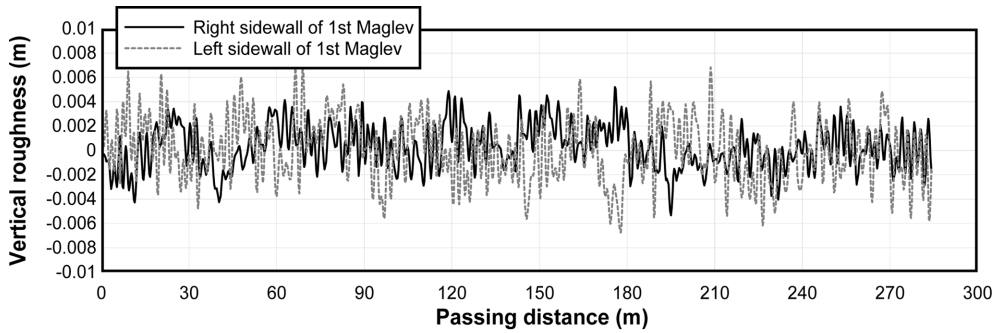
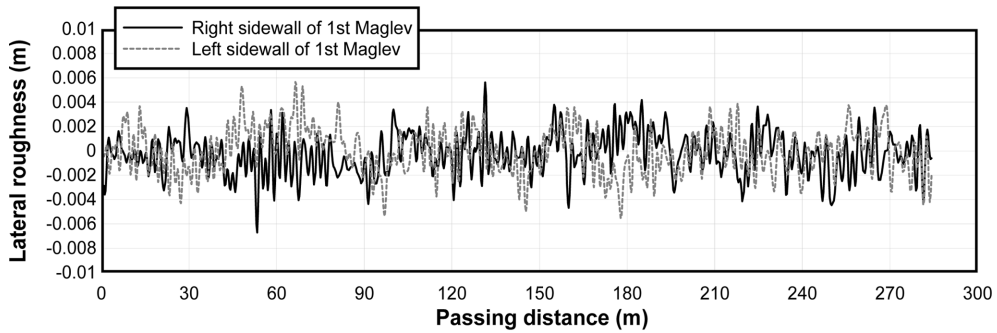


Fig. 10 PSD function to generate the roughness in the sidewall



(a) Vertical roughness profile



(b) Lateral roughness profile

Fig. 11 Roughness profile in the sidewall

5. Maglev train-guideway interaction

When Maglev train moves on guideways, the interaction force additional to static force is produced due to the restoration of the levitation and guidance force between SCM and guideways. The coupling terms between DOF of Maglev train and guideway structures in composing the system matrices of Maglev train-guideway system are formed by considering the interactive force between SCM and guideways. The interactive force means the reaction force, which is resulted from the deformation of the equivalent spring to model the levitation and guidance force between SCM and guideways.

Eight pieces of SCM are installed in each bogie. The interaction force between the first SCM ($j1$) of the j -th bogie and guideway is given as Eqs. (4) and (5).

$$F_{bz}^{j1} = \frac{1}{16} M_s^{j1} g + K_{ss} R_{rz}^{j1} \quad (4)$$

$$F_{bx}^{j1} = K_{nn} R_{rx}^{j1} \quad (5)$$

where M_s^{j1} is the sprung mass of the $j1$ -SCM, and R_{rz} and R_{rx} are the relative deformations between $j1$ -SCM and guideway in vertical and lateral direction (Appendix A). K_{ss} and K_{nn} are the equivalent spring constants to compensate for the restoring force of the levitation and guidance force in vertical and lateral direction. The equivalent spring constants are the variables of the Maglev train speed (V), i.e., $K_{ss} = f_z(V)$ and $K_{nn} = f_x(V)$ as given in Eqs. (6) and (7) (Ohashi *et al.* 1998).

$$f_z(V) = 5.43 \times EXP(-6.18/V) \quad (\text{MN/m}) \quad (6)$$

$$f_x(V) = 2.75 \times EXP(-14.5/V) \quad (\text{MN/m}) \quad (7)$$

where $EXP(\cdot)$ is the exponential function.

In modeling the sidewalls with beam elements, the vertical and lateral interactive force as shown in Eqs. (4) and (5) are transferred to the nodes of the finite element mesh by interpolation. Then, the equations of motion of guideway structures are given as Eq. (8).

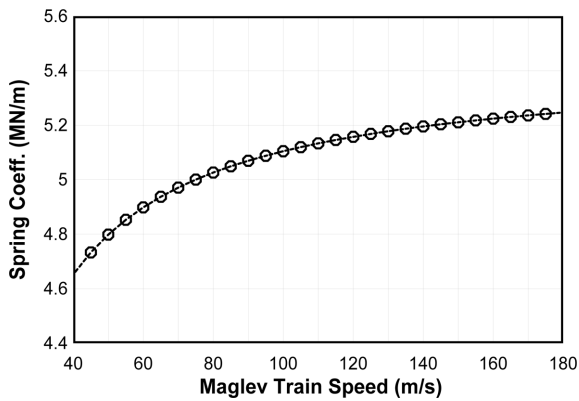


Fig. 12 Vertical equivalent spring coefficient $f_z(V)$ according to the speed of Maglev train

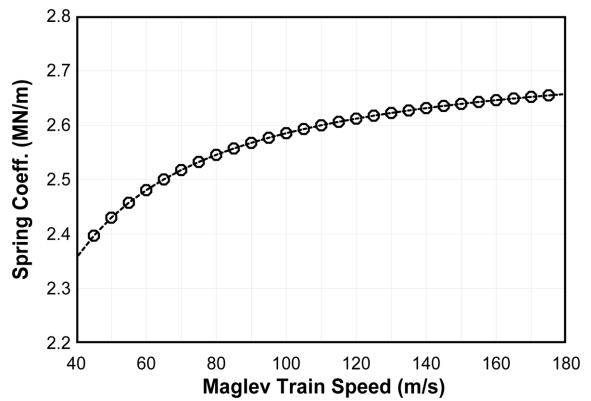


Fig. 13 Lateral equivalent spring coefficient $f_x(V)$ according to the speed of Maglev train

$$[M_b]\{\ddot{q}_b(t)\} + [C_b]\{\dot{q}_b(t)\} + [K_b]\{q_b(t)\} = \{F_b(t)\} \tag{8}$$

where $[K_b], [C_b], [M_b]$, and $\{q_b(t)\}$ are the mass matrix, damping matrix, stiffness matrix, and vector of nodal DOF of guideway structures, respectively and $\{F_b(t)\}$ is the load vector transferred to the nodes.

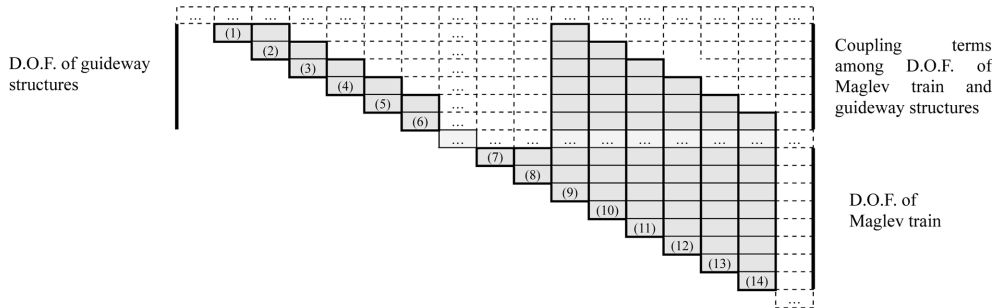
From the foregoing Eqs. (1), (4), (5), and (8), the equation of motion of the Maglev train-guideway structure system is derived as

$$[M_{total}(t)]\{\ddot{q}(t)\} + [C_{total}(t)]\{\dot{q}(t)\} + [K_{total}(t)]\{q(t)\} = \{P_{total}(t)\} \tag{9}$$

in the other form,

$$\begin{bmatrix} M_b & 0 \\ 0 & M_v \end{bmatrix} \begin{Bmatrix} \ddot{q}_b(t) \\ \ddot{q}_v(t) \end{Bmatrix} + \begin{bmatrix} C_b & 0 \\ 0 & C_v \end{bmatrix} \begin{Bmatrix} \dot{q}_b(t) \\ \dot{q}_v(t) \end{Bmatrix} + \begin{bmatrix} K_b + K_p(t) & K_c(t) \\ K_c^T(t) & K_v \end{bmatrix} \begin{Bmatrix} q_b(t) \\ q_v(t) \end{Bmatrix} = \begin{Bmatrix} P_b(t) \\ P_v(t) \end{Bmatrix} \tag{10}$$

where $[M_{total}(t)], [C_{total}(t)]$, and $[K_{total}(t)]$ are respectively the mass matrix, damping matrix, and stiffness matrix of the Maglev-guideway structure system which vary with time as these matrices are determined by the positions of SCM. $\{P_{total}(t)\}$ is the load vector and $\{q(t)\} = \langle q_b(t) \ q_v(t) \rangle^T$ is the vector composed of nodal DOF of guideway structure and DOF of SCM, bogies, and carbodies. $[M_{total}(t)]$ is composed of the mass matrices of guideway structures ($[M_b]$) and mass matrices of Maglev train ($[M_v]$). $[C_{total}(t)]$ is composed of the damping matrices of guideway



- (1) D.O.F. of the nodes connected to the 1st SCM
- (2) D.O.F. of the nodes connected to the 2nd SCM
- (3) D.O.F. of the nodes connected to the 3rd SCM
- (4) D.O.F. of the nodes connected to the 4th SCM
- (5) D.O.F. of the nodes connected to the 5th SCM
- (6) D.O.F. of the nodes connected to the 6th SCM
- (7) D.O.F. of all carbodies
- (8) D.O.F. of all bogies
- (9) D.O.F. of the 1st SCM
- (10) D.O.F. of the 2nd SCM
- (11) D.O.F. of the 3rd SCM
- (12) D.O.F. of the 4th SCM
- (13) D.O.F. of the 5th SCM
- (14) D.O.F. of the 6th SCM

Fig. 14 Storage scheme of system matrices by skyline algorithm

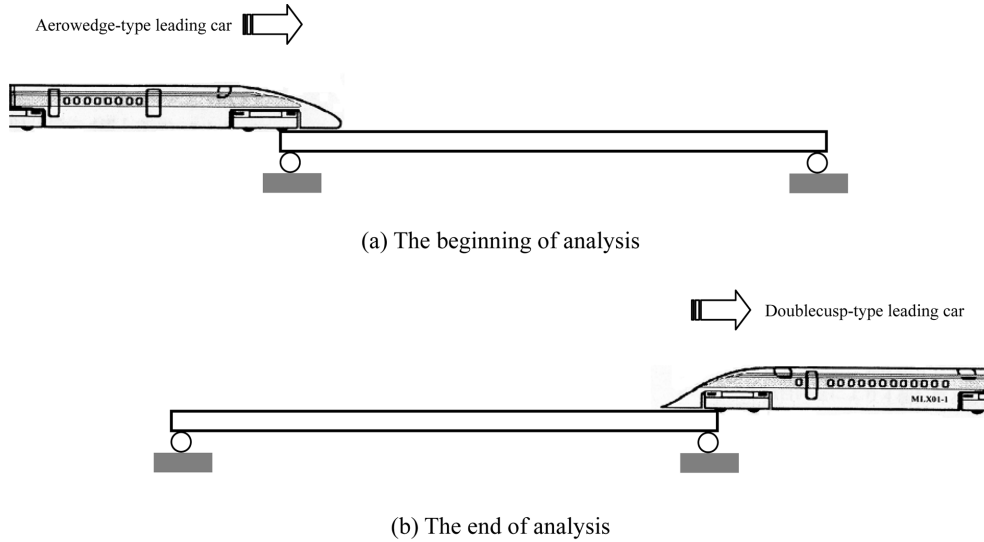


Fig. 15 Total running time of analysis

structures ($[C_b]$) and damping matrices of Maglev train ($[C_v]$). $[K_{total}(t)]$ is composed of the stiffness matrices of guideway structures ($[K_b]$), stiffness matrices of Maglev train ($[K_v]$), stiffness matrices for equivalent spring of the levitation and guidance force $[K_p(t)]$, and stiffness matrices of coupling terms among the DOF of Maglev train and guideway structures ($[K_c(t)]$). $[K_c(t)]$ is composed by considering the relative relation between the DOF of SCM and guideway structures. The load vector $\{P_{total}(t)\}$ consists of the contributions to guideway structures ($\{P_b(t)\}$) and Maglev train ($\{P_v(t)\}$). As a result, all the system matrices of Maglev train-guideway structure system are composed.

To obtain the numerical solution for the equations of motion of Maglev train-guideway structure system, Newmark's β method with average acceleration ($\gamma=1/2$ and $\beta=1/4$), which is unconditionally stable, is used. As shown in Eq. (10), there exist the coupling terms between the DOF of Maglev train and guideway structures in the system matrices. Because the coupling terms are differently composed as the position of SCM as time step, the storage scheme using skyline algorithm as shown in Fig. 14 is used to store the system matrices efficiently in computer memory units. Total running time of analysis is the interval from the arrival of a leading aerowedge-type car until the leaving of a doublecusp-type leading car as shown in Fig. 15.

6. Numerical examples

The proposed dynamic analysis system of guideway structures considering ultra high-speed Maglev train-guideway interaction is verified through the exemplificative numerical analyses.

In the real guideway structures constructed in Japan, the sub-structure of a bridge is the simply supported PC (pre-stressed concrete) box girder with 37.8m-span, which is continuously arranged to form the total bridge section. The guideways, which are the sidewalls of the inverted-T shaped type in Japan, are constructed on the bridge. The levitation, guidance, and propulsion coils are installed

in these sidewalls.

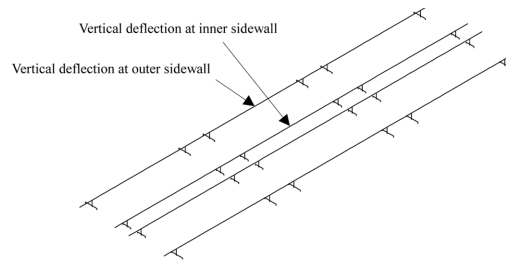
In this analysis, the three sidewalls with 12.6m-span are set up longitudinally on the bridge. The structural properties of the bridge and sidewall for the analysis are given in Fig. 7, Tables 3, and 4 (Sogabe *et al.* 2003). MLX-01 of Japanese Maglev train has three-car formation and five-formation, and MLX-01 with five-car formation is applied in this analysis.

Table 3 Material properties of the bridge for the analysis

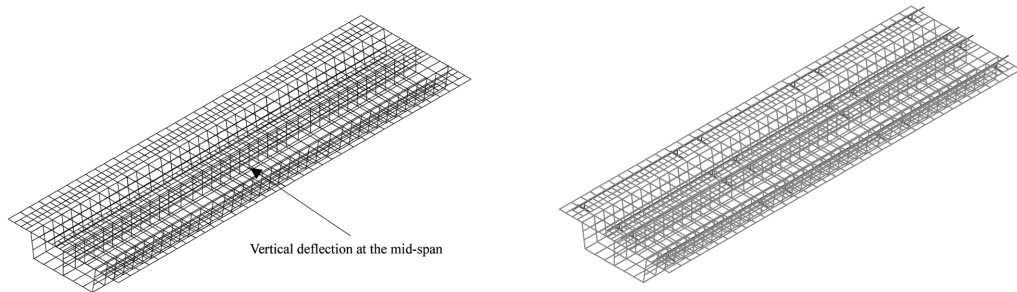
Terms	Unit	Value
Concrete	Young's modulus	kN/m^2
	Poisson's ratio	-
	Specific weight	t/m^3
Damping ratio	%	

Table 4 Structural properties of the sidewall for the analysis

Terms	Unit	Value
Young's modulus	kN/m^2	3.3×10^7
Area	m^2	0.4461
Horizontal moment of inertia	m^4	0.0172
Vertical moment of inertia	m^4	0.0710
Additional dead load (coil etc.)	kN/m	2.533



(a) Guideways : 432 beam elements



(b) Guideway structures : 1260(4-node NFS elements) + 288(5-node NFS elements)

(c) Full model

Fig. 16 Three-dimensional finite element model of guideway structures and data points of analysis results

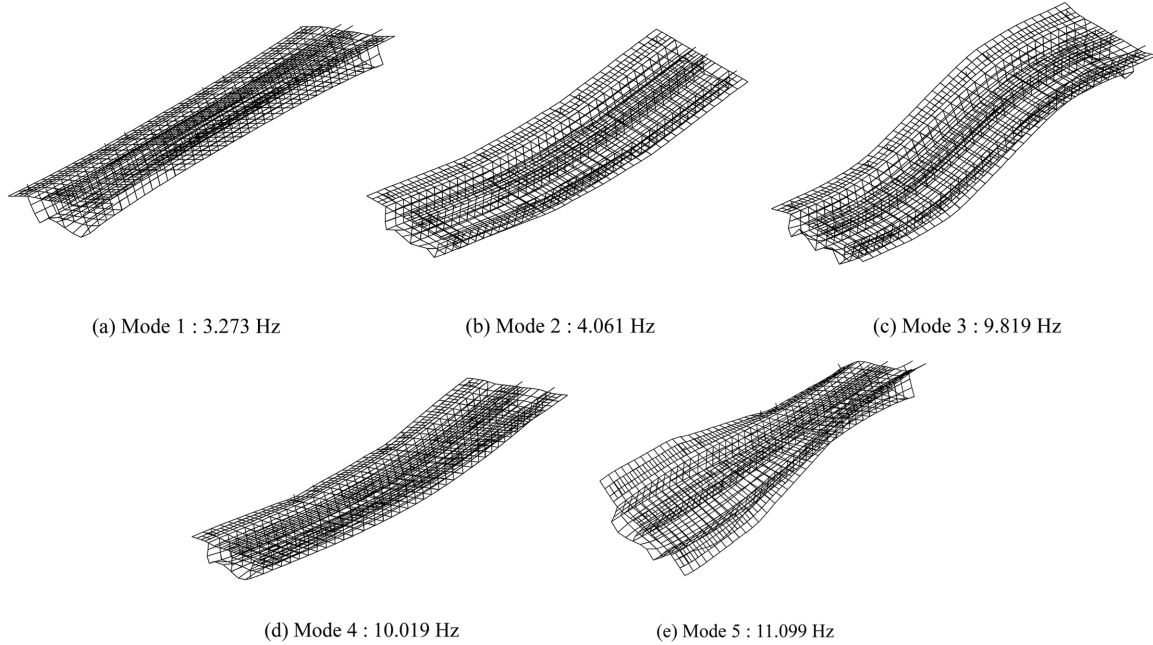


Fig. 17 Natural vibration modes and frequencies of guideway structures

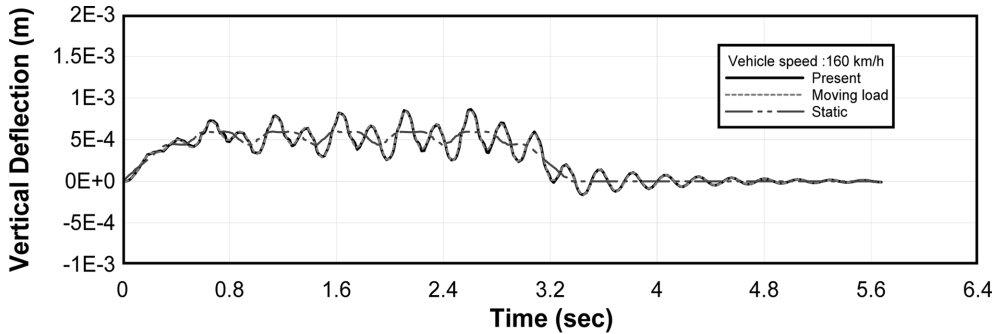
Table 5 Critical Maglev train speed for each mode

Mode No.	Critical speed (km/h)
1	255
2	316
3	764
4	779
5	863

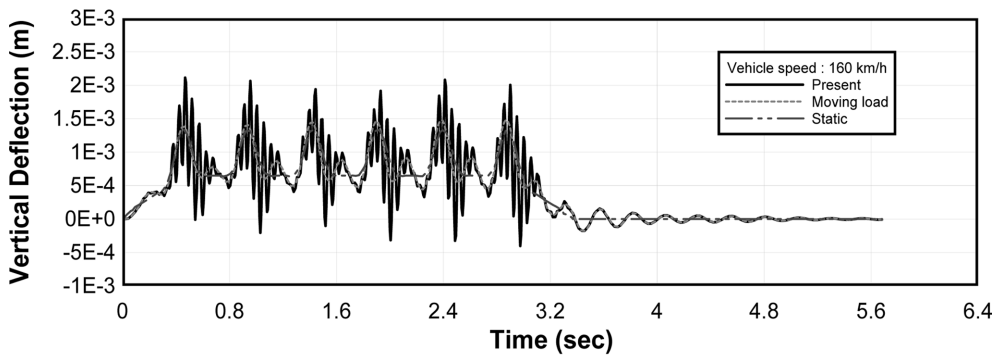
The vertical deflections at the mid-span of the sidewalls and bridge are observed as analysis results (Fig. 16). The natural vibration frequencies and modes of guideway structures are shown in Fig. 17, which are in close connection with the resonance phenomena of guideway structures when Maglev train passes. The relation between the critical speed of Maglev train (V_{cr}) and natural frequencies of guideway structures can be expressed as Eq. (11). The critical speed of Maglev train means the speed of Maglev train, which makes resonance phenomena of guideway structures occur.

$$V_{cr} = 3.6 \times \omega \times d \text{ (km/h)} \quad (11)$$

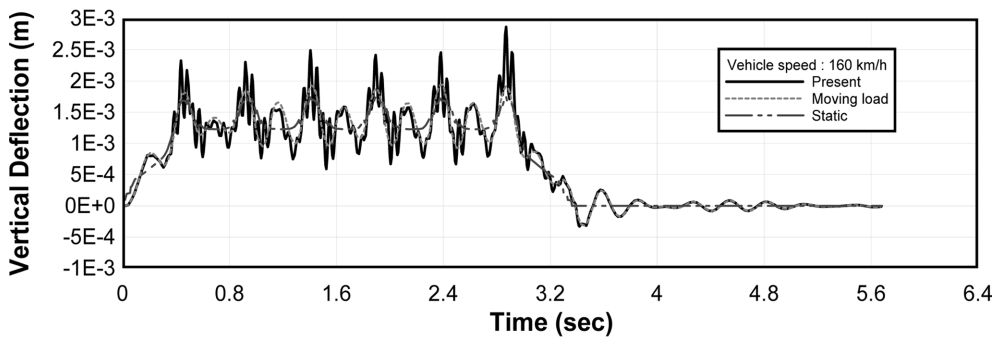
where ω is the natural frequency of the guideway structure and d is the effective beating interval, which is 21.6 m in this analysis. The beating interval means the distance between the fore bogie and rear bogie of a carbody. By the foregoing Eq. (11), the critical speed for each mode of the guideway structure is given as Table 5.



(a) Data point at the mid-span of the bridge



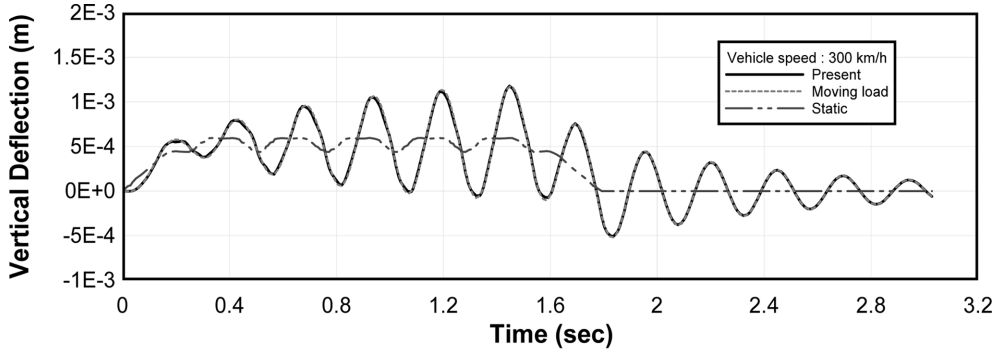
(b) Data point at the mid-span of the inner sidewall



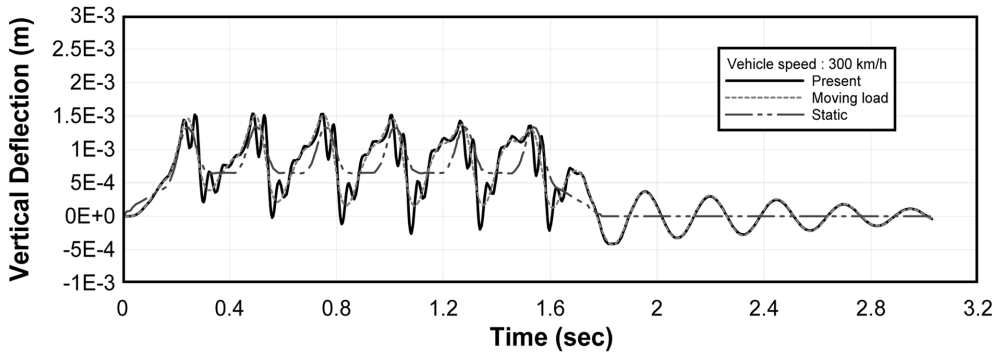
(c) Data point at the mid-span of the outer sidewall

Fig. 18 Time histories of vertical deflections ($V = 160$ km/h)

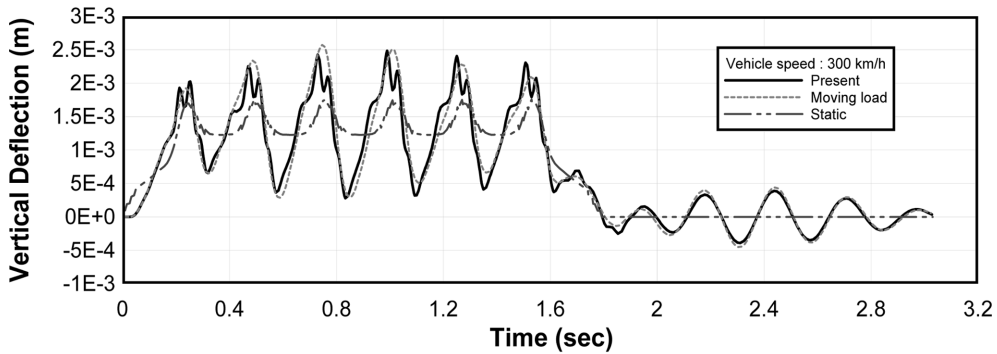
Maglev train moves by wheels at the speed under 160 km/h and it moves by the aid of the magnetic force at the speed over 160 km/h. Therefore, the objective speed of Maglev train in this analysis is chosen as 160, 300, and 550 km/h. Analysis results for each speed of Maglev train are compared with those of moving load and static analysis as shown in Figs. 18, 19, 20, and 21. In the analysis case of 160 km/h, it is known that the vibration of guideway structures is sensitively influenced by the roughness of sidewalls and vibration of Maglev train as shown in Fig. 18. In the analysis case of 300 km/h, because the speed is close to the critical speed of 316 km/h for Mode 2,



(a) Data point at the mid-span of the bridge



(b) Data point at the mid-span of the inner sidewall

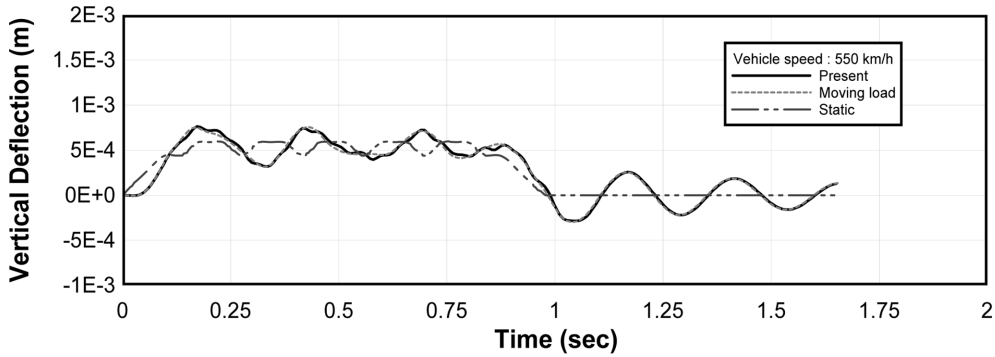


(c) Data point at the mid-span of the outer sidewall

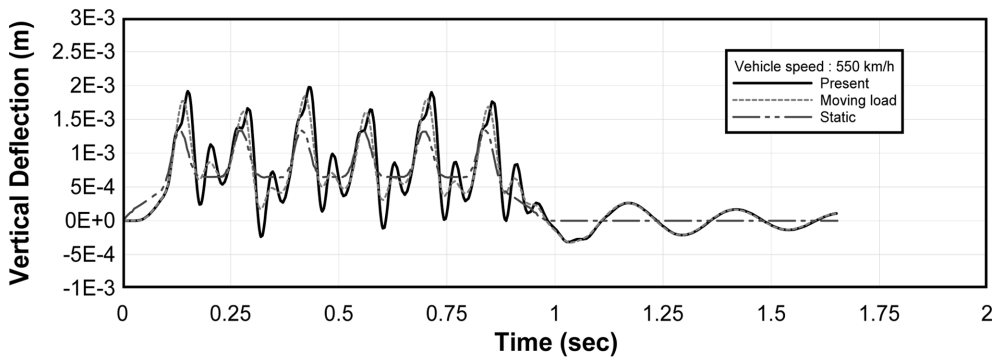
Fig. 19 Time histories of vertical deflections ($V = 300$ km/h)

the resonance phenomena of guideway structures come into existence as shown in Fig. 19. In the analysis case of 550 km/h, which is the maximum speed of Maglev train, the difference of analysis results with moving load analysis is observed as shown in Figs. 20 and 21, which is the same tendency as shown in the analysis results of other speeds.

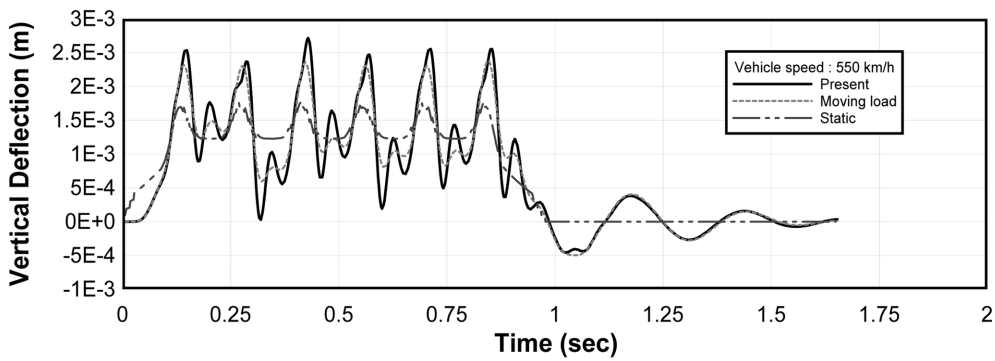
Judging from the comparison of all analysis results, it is known that the analysis results in this study have the obvious difference with those of moving load and static analysis. The analysis results



(a) Data point at the mid-span of the bridge



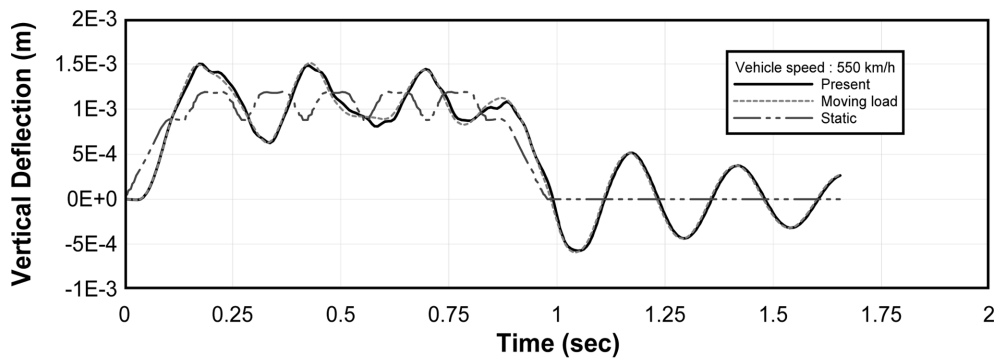
(b) Data point at the mid-span of the inner sidewall



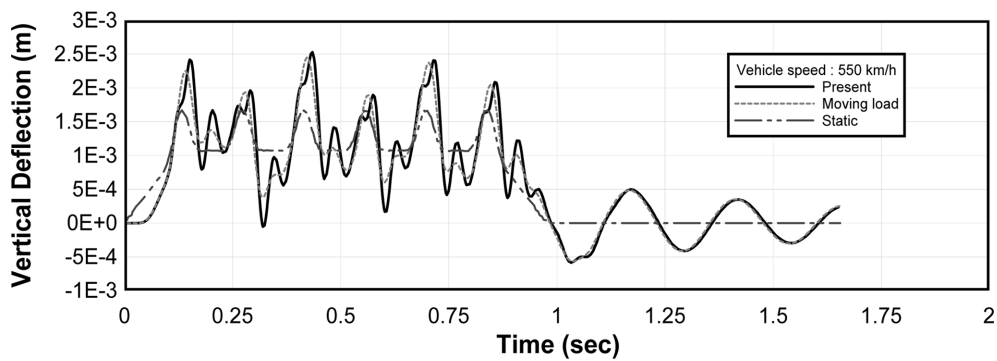
(c) Data point at the mid-span of the outer sidewall

Fig. 20 Time histories of vertical deflections ($V = 550$ km/h)

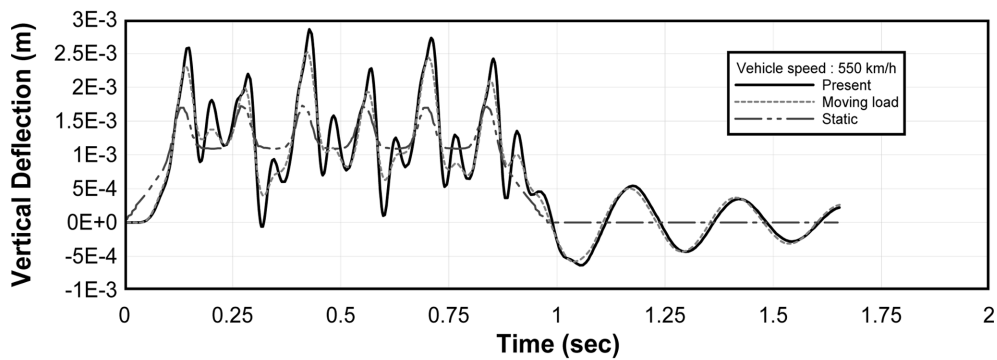
at the mid-span of the bridge are not so much different from those of moving load analysis. However, the analysis results at the mid-span of the inner and outer sidewalls are very different from those of moving load analysis. Therefore, by using the dynamic analysis system proposed in this study, it is possible to analyze accurately the sidewalls, which are the important structural constituents in guideway structures.



(a) Data point at the mid-span of the bridge



(b) Data point at the mid-span of the inner sidewall



(c) Data point at the mid-span of the outer sidewall

Fig. 21 Time histories of vertical deflections ($V = 550$ km/h) : 2 trains

7. Conclusions

In this study, the new three-dimensional finite element analysis model for the dynamic analysis of guideway structures considering ultra high-speed Maglev train-guideway interaction, was proposed. As a numerical example, the simply supported PC box-girder bridge was analyzed by the present study. Judging from the analysis results, the conclusions as following can be obtained.

(1) Although it takes much time to make the input data of three-dimensional guideway structures to use the dynamic analysis system proposed in this study, it is possible to analyze the dynamic behavior of the specific structural constituents of guideway structures. In addition, it is possible to model efficiently the connecting part of the sidewalls and sub-structures by using the variable-node NFS finite element.

(2) In the existing three-dimensional train-bridge interaction analysis methods, the position of a train in each time step is calculated and the equations of motion of a bridge are solved after calculating the interactive force between the train and bridge from the assumed deflections of a bridge. The above-mentioned computations are repeated to obtain the final solution of equations of motion of a bridge, until the difference between the assumed deflections and the solved deflections of a bridge is smaller than a certain tolerance. On the other hand, in this study, the equations of motion of Maglev train-guideway structure system are directly composed and solved in each time step. Therefore, it is possible to obtain efficiently the solution of the deflections of guideway structures without the repetition of computations.

(3) Judging from the analysis results of the simply supported PC box-girder bridge, there is the obvious difference between the analysis results of the present study and moving load analysis. As a result, for the accurate and efficient analysis of the dynamic behavior of guideway structures, the three-dimensional finite element analysis system proposed in this study must be used.

(4) In the prospective construction of guideway structures, by applying the three-dimensional finite element analysis system proposed in this study, it is possible to grasp the characteristics of the dynamic behavior, to evaluate the dynamic serviceability and safety, and to estimate fatigue life of guideway structures.

Acknowledgements

The research was supported by the Postdoctoral Fellowship Program of Japan Society for the Promotion of Science. The first author will forever grateful to the host of Japan Society for the Promotion of Science and the second author, Professor Yozo FUJINO in the University of Tokyo.

References

- Azakami, M. (1996), "The development of Maglev bogie system on the first train set for Yamanashi test line", *RTRI Report*, **10**(1), 11-16.
- Choi, C.K., Chung, K.Y. and Lee, T.Y. (2001), "A direct integration method for strains due to nonconforming modes", *Struct. Eng. Mech.*, **11**(3), 325-340.
- Esveld, C. (2001), *Modern Railway Track*, Second Ed., MRT-Productions, The Netherlands.
- Garg, V.K. and Dukkipati, R.V. (1984), *Dynamics of Railway Vehicle Systems*, Academic Press, Canada.
- Higashi, K., Ohashi, S., Ohsaki, H. and Masada, E. (1999), "Magnetic damping of the electrodynamic suspension-type superconducting levitation system", *Electr. Eng. JPN*, **127**(2), 49-60.
- Kim, S.H. (1997), *Introduction to the Railway System*, Jajak Academy, Korea Republic.
- Kim, S.I., Kwark, J.W. and Chang, S.P. (1999), "Bridge/train interaction analysis using 3-dimensional articulated high-speed train model", *J. Korean Soc. Civil Eng.*, **19**(1-4), 505-516.
- Kwark, J.W., Choi, E.S., Kim, Y.J., Kim, B.S. and Kim, S.I. (2004), "Dynamic behavior of two-span continuous concrete bridges under moving high-speed train", *Comput. Struct.*, **82**, 463-474.
- Matsudaira, Y. and Takao, K. (1994), "Development of bodies and nose-shape of head cone for vehicles on

- yamanashi test line”, *RTRI Report*, **8**(10), 7-12.
- Matsuura, A., Hashimoto, S. and Furukawa, A. (1994), “Relation between riding quality of maglev vehicle and guideway construction accuracy”, *J. Japan Soc. Civil Eng.*, **48**(IV-22), 67-76.
- Ohashi, S., Ohsaki, H. and Masada, E. (1998), “Equivalent model of the side wall electrodynamic suspension system”, *Electr. Eng. JPN*, **124**(2), 95-105.
- Ohashi, S., Ohsaki, H. and Masada, E. (2000), “Running characteristics of the superconducting magnetically levitated train in the case of superconducting coil quenching”, *Electr. Eng. JPN*, **130**(1), 63-73.
- Park, H.S. (1999), *Dynamic Analysis of Bridges using Advanced High-speed Railway Vehicle Models*, Ph.D. Thesis, Department of Civil Engineering, Seoul National University, Korea Republic.
- Sogabe, M., Matsumoto, N., Tanabe, M., Fujino, Y., Wakui, H. and Ueno, M. (2003), “A study on dynamic interaction analysis for maglev vehicle and guideway structures”, *J. Japan Soc. Civil Eng.*, **73**(I-63), 119-134.
- Song, M.K. and Choi, C.K. (2001), “Analysis of high-speed vehicle-bridge interactions by a simplified 3-D model”, *Struct. Eng. Mech.*, **13**(5), 505-532.
- Song, M.K., Noh, H.C. and Choi, C.K. (2003), “A new three-dimensional finite element analysis model of high-speed train-bridge interactions”, *Eng. Struct.*, **25**(13), 1611-1626.
- Takao, K., Yoshimura, M., Tagawa, N., Matsudaira, Y., Nagano, K. and Inoue, A. (1996), “Development of the superconducting Maglev Vehicles on the Yamanashi test line”, *RTRI Report*, **10**(1), 5-10.
- Tanabe, M., Wakui, H. and Matumoto, N. (1997), DIASTARS-Dynamic Interaction Analysis for Shinkansen Train and Railway Structure. *Proceedings of WCRR '97*, Firenze, November 16-19.
- Xia, H., Zhang, N. and De Roeck, G. (2003), “Dynamic analysis of high-speed railway bridge under articulated trains”, *Comput. Struct.*, **63**(3), 511-523.
- Yoshioka, H. (1988), “Dynamic model of Maglev vehicle”, *RTRI Report*, **2**(6), 17-22.
- Yoshioka, H., Suzuki, E., Seino, H., Azakami, M., Oshima, H. and Nakanishi, T. (1998), “Characteristics of the dynamics of the MLX01 Yamanashi Maglev test line vehicles”, *RTRI Report*, **12**(8), 21-34.

Appendix A. Equations of motion of Maglev train model

A.1 Equations of motion of the aerowedge-type leading car with twenty-four DOF

The equations of motion for the aerowedge-type leading car can be derived by substituting the equations, which define the kinetic energy (E_k), potential energy (E_p), and damping energy (E_d) of the aerowedge-type leading car, for Lagrange's equations of Eq. (1). To apply the Lagrange's equations of motion, E_k , E_p , and E_d for the Maglev train model with 24 DOF as shown in Figs. 5 and 6 are defined as follow;

(1) Kinetic energy (E_k)

$$\begin{aligned}
 E_k = & \frac{1}{2} \{ m_c (\dot{x}_c^2 + \dot{y}_c^2 + \dot{z}_c^2) + (I_{xc} \dot{\theta}_c^2 + I_{yc} \dot{\phi}_c^2 + I_{zc} \dot{\psi}_c^2) \} \\
 & + \frac{1}{2} \sum_{i=1}^2 \{ m_{ti} (\dot{x}_{ti}^2 + \dot{y}_{ti}^2 + \dot{z}_{ti}^2) + (I_{xti} \dot{\theta}_{ti}^2 + I_{yti} \dot{\phi}_{ti}^2 + I_{zti} \dot{\psi}_{ti}^2) \} \\
 & + \frac{1}{2} \sum_{i=1}^2 \{ m_{si} \dot{z}_{si}^2 + (I_{xsi} \dot{\theta}_{si}^2 + I_{ysi} \dot{\phi}_{si}^2) \}
 \end{aligned} \tag{A.1}$$

(2) Potential energy (E_p)

$$E_p = \frac{1}{2} \left[\sum_{i=1}^8 K_{sxi} R_{Ksxi}^2 + \sum_{i=1}^8 K_{syi} R_{Ksyi}^2 + \sum_{i=1}^8 K_{szi} R_{Kszi}^2 + \sum_{i=1}^8 K_{bsxi} R_{Kbsxi}^2 \right]$$

$$\begin{aligned}
& + \sum_{i=1}^8 K_{bsyi} R_{Kbsyi}^2 + \sum_{i=1}^4 K_{yawwi} R_{Kyawwi}^2 + \sum_{i=1}^2 K_{gxi} R_{gxi}^2 + \sum_{i=1}^8 K_{pzi} R_{pzi}^2 \\
& + \left[\sum_{i=1}^{16} K_{mri} R_{mri}^2 + \sum_{i=1}^{16} K_{sri} R_{sri}^2 + \sum_{i=1}^{16} K_{nsri} R_{nsri}^2 + \sum_{i=1}^{16} K_{ssi} R_{ssi}^2 \right]
\end{aligned} \quad (\text{A.2})$$

(3) Damping energy (E_d)

$$E_d = \frac{1}{2} \sum_{i=1}^8 D_{szi} \dot{D}_{Dszi}^2 \quad (\text{A.3})$$

For the definition of E_p and E_d , the relative deformations of the springs and dampers of suspensions should be defined. For the Maglev train model with 24 DOF as shown in Figs. 5 and 6, the relative deformations are as follow.

(4) $R_{Ksxi}, R_{Ksyi}, R_{Kszi}, R_{Kbsyi}, R_{Dszi}$ ($i = 1 \sim 8$)

For $i = 1, 2$

$$R_{Ksxi} = (-1)^i (x_{c1} - x_{il} + h_1 \phi_c + h_2 \phi_{il}) + (-1)^{m+1} (L_l + d_1) \varphi_{c1} \quad (\text{A.4})$$

$$R_{Ksyi} = (-1)^l (y_{c1} - y_{il} - h_1 \theta_{c1} - h_2 \theta_{il}) + (-1)^{m+1} e_2 (\varphi_{c1} - \varphi_{il}) \quad (\text{A.5})$$

$$R_{Kszi} = z_{c1} - z_{il} + (-1)^{l+1} (L_l + d_1) \theta_{c1} + (-1)^{i+1} e_1 (\phi_{c1} - \varphi_{il}) \quad (\text{A.6})$$

$$R_{Kbsyi} = (-1)^l (y_{c1} - y_{il} - (h_1 - h_{bs}) \theta_{c1} - (h_2 - h_{bs}) \theta_{il}) + (-1)^{m+1} e_3 (\varphi_{c1} - \varphi_{il}) \quad (\text{A.7})$$

$$R_{Dszi} = R_{Kszi} \quad (\text{A.8})$$

where $l = \text{integer}[(i+1)/2]$ and $m = \text{integer}[(i+2)/2]$.

For $i = 3 \sim 6$

$$R_{Ksxi} = (-1)^i (x_{c1} - x_{il} + h_1 \phi_{c1} + h_2 \phi_{il}) + (-1)^{m+1} (L_l - d_1) \varphi_{c1} \quad (\text{A.9})$$

$$R_{Ksyi} = (-1)^l (y_{c1} - y_{il} - h_1 \theta_{c1} - h_2 \theta_{il}) + (-1)^{m+1} e_2 (\varphi_{c1} - \varphi_{il}) \quad (\text{A.10})$$

$$R_{Kszi} = z_{c1} - z_{il} + (-1)^{l+1} (L_l - d_1) \theta_{c1} + (-1)^{i+1} e_1 (\phi_{c1} - \varphi_{il}) \quad (\text{A.11})$$

$$R_{Kbsyi} = (-1)^l (y_{c1} - y_{il} - (h_1 - h_{bs}) \theta_{c1} - (h_2 - h_{bs}) \theta_{il}) + (-1)^{m+1} e_3 (\varphi_{c1} - \varphi_{il}) \quad (\text{A.12})$$

$$R_{Dszi} = R_{Kszi} \quad (\text{A.13})$$

where $l = \text{integer}[(i+3)/4]$ and $m = \text{integer}[(i+2)/2]$.

For $i = 7, 8$

$$R_{Ksxi} = (-1)^i (x_{c2} - x_{il} + h_1 \phi_{c2} + h_2 \phi_{il}) + (-1)^{m+1} (L_{l-1} - d_1) \varphi_{c2} \quad (\text{A.14})$$

$$R_{Ksyi} = (-1)^{l+1} (y_{c2} - y_{il} - h_1 \theta_{c2} - h_2 \theta_{il}) + (-1)^{m+1} e_2 (\varphi_{c2} - \varphi_{il}) \quad (\text{A.15})$$

$$R_{Kszi} = z_c - z_{il} + (-1)^{l+1} (L_{l-1} - d_1) \theta_{c2} + (-1)^{i+1} e_1 (\phi_{c2} - \varphi_{il}) \quad (\text{A.16})$$

$$R_{Kbsyi} = (-1)^{l+1} (y_{c2} - y_{il} - (h_1 - h_{bs}) \theta_{c2} - (h_2 - h_{bs}) \theta_{il}) + (-1)^{m+1} e_3 (\varphi_{c2} - \varphi_{il}) \quad (\text{A.17})$$

$$R_{Dszi} = R_{Kszi} \quad (\text{A.18})$$

where $l = \text{integer}[(i+1)/4]$ and $m = \text{integer}[(i+8)/8]$.

(5) R_{Kbsxi}, R_{Kyawi} ($i = 1\sim 4$)

$$R_{Kbsx1} = -(x_{c1} - x_{t1} + (h_1 + h_2 - h_{bs})\phi_{c1} + h_{bs}\phi_{t1}) - (L_1 + d_1)\varphi_{c1} \quad (\text{A.19})$$

$$R_{Kyaw1} = \frac{x_{c1}}{(h_1 + h_{yaw})} + \frac{x_{t1}}{(h_2 - h_{yaw})} \quad (\text{A.20})$$

For $i = 2, 3$

$$R_{Kbsxi} = (-1)^i(x_{c1} - x_{tl} + (h_1 + h_2 - h_{bs})\phi_{c1} + h_{bs}\phi_{tl}) + (-1)^{m+1}(L_l - d_1)\varphi_{c1} \quad (\text{A.21})$$

$$R_{Kyawl} = \frac{x_{c1}}{(h_1 + h_{yaw})} + \frac{x_{tl}}{(h_2 - h_{yaw})} \quad (\text{A.22})$$

where $l = \text{integer}[(i + 1)/2]$ and $m = \text{integer}[(i + 2)/2]$.

$$R_{Kbsx4} = (x_{c2} - x_{t2} + (h_1 + h_2 - h_{bs})\phi_{c2} + h_{bs}\phi_{t2}) - (L_1 + d_1)\varphi_{c2} \quad (\text{A.23})$$

$$R_{Kyaw4} = \frac{x_{c2}}{(h_1 + h_{yaw})} + \frac{x_{t2}}{(h_2 - h_{yaw})} \quad (\text{A.24})$$

(6) R_{Kgx1} ($i = 1, 2$)

$$K_{Kgx1} = (y_{c1} + (h_4 + h_5 - h_1 - h_2)\theta_{c1}) - (y_{c2} + (h_4 + h_5 - h_1 - h_2)\theta_{c2}) \quad (\text{A.25})$$

$$K_{Kgx2} = -(y_{c1} + (h_5 - h_1 - h_2)\theta_{c1}) + (y_{c2} + (h_5 - h_1 - h_2)\theta_{c2}) \quad (\text{A.26})$$

(7) R_{Kpzi} ($i = 1\sim 8$)

$$R_{pzi} = z_{tn} - z_{sn} + (-1)^{q+1}d_2\theta_{tn} + (-1)^{i+1}b_u(\phi_{tn} - \phi_{sn}) \quad (\text{A.27})$$

where $n = \text{integer}[(i + 3)/4]$ and $q = \text{integer}[(i + 1)/2]$.(8) R_{rx1}, R_{rzi} ($i = 1\sim 16$)For $i = 1, 8$

$$R_{rx1} = (-1)^i(r\phi_{sq} - G_{rx} - u_{bi}) \quad (\text{A.28})$$

$$R_{rzi} = z_{sq} + (-1)^{i+1}b_r\phi_{sq} - \frac{(5-2v)}{2}a\theta_{sq} - G_{rz} - w_{bi} \quad (\text{A.29})$$

where $q = \text{integer}[(i + 7)/8]$ and $v = \text{integer}[(i + 1)/2]$.For $i = 9\sim 16$, $v = \text{integer}[(i + 1)/2] - 4$, and u_b and w_b are the deflection of a bridge in lateral and vertical direction.By the same way, the equations of motion for the doublecusp-type leading and intermediate cars can be derived by substituting the equations, which define the kinetic energy (E_k), potential energy (E_p), and damping energy (E_d) of the doublecusp-type leading and intermediate cars, for Lagrange's equations.